

PAPER

# The mechanical property and microscopic deformation mechanism of nanoparticle-contained graphene foam materials under uniaxial compression

To cite this article: Muhammad Bilal Khan *et al* 2021 *Nanotechnology* **32** 115701

View the [article online](#) for updates and enhancements.

## You may also like

- [Nanoarchitected CNTs-Grafted Graphene Foam with Hierarchical Pores as a Binder-Free Cathode for Lithium-Oxygen Batteries](#)  
Weihua Wan, Xingbao Zhu, Xianglei He et al.
- [Microscopic deformation mechanism and main influencing factors of carbon nanotube coated graphene foams under uniaxial compression](#)  
Shuai Wang, Chao Wang, Muhammad Bilal Khan et al.
- [High porosity and light weight graphene foam heat sink and phase change material container for thermal management](#)  
Abdelhafid Zehri, Majid Kabiri Samani, Martí Gutierrez Latorre et al.



The Electrochemical Society  
Advancing solid state & electrochemical science & technology

242nd ECS Meeting

Oct 9 – 13, 2022 • Atlanta, GA, US

Abstract submission deadline: **April 8, 2022**

Connect. Engage. Champion. Empower. Accelerate.

**MOVE SCIENCE FORWARD**



Submit your abstract



# The mechanical property and microscopic deformation mechanism of nanoparticle-contained graphene foam materials under uniaxial compression

Muhammad Bilal Khan<sup>1,2</sup> , Chao Wang<sup>3,4,\*</sup> , Shuai Wang<sup>1,2</sup>,  
Daining Fang<sup>1,2</sup> and Shaohua Chen<sup>1,2,\*</sup>

<sup>1</sup>Institute of Advanced Structure Technology, Beijing Institute of Technology, Beijing 100081, People's Republic of China

<sup>2</sup>Beijing Key Laboratory of Lightweight Multi-functional Composite Materials and Structures, Beijing Institute of Technology, Beijing, 100081, People's Republic of China

<sup>3</sup>LNM, Institute of Mechanics, Chinese Academy of Sciences, Beijing 100190, People's Republic of China

<sup>4</sup>School of Engineering Science, University of Chinese Academy of Sciences, Beijing, 100049, People's Republic of China

E-mail: [wangchao@lnm.imech.ac.cn](mailto:wangchao@lnm.imech.ac.cn) and [shchen@bit.edu.cn](mailto:shchen@bit.edu.cn)

Received 23 August 2020, revised 19 September 2020

Accepted for publication 2 December 2020

Published 23 December 2020



CrossMark

## Abstract

Nanoparticle-contained graphene foams have found more and more practical applications in recent years, which desperately requires a deep understanding on basic mechanics of this hybrid material. In this paper, the microscopic deformation mechanism and mechanical properties of such a hybrid material under uniaxial compression, that are inevitably encountered in applications and further affect its functions, are systematically studied by the coarse-grained molecular dynamics simulation method. Two major factors of the size and volume fraction of nanoparticles are considered. It is found that the constitutive relation of nanoparticle filled graphene foam materials consists of three parts: the elastic deformation stage, deformation with inner re-organization and the final compaction stage, which is much similar to the experimental measurement of pristine graphene foam materials. Interestingly, both the initial and intermediate modulus of such a hybrid material is significantly affected by the size and volume fraction of nanoparticles, due to their influences on the microstructural evolution. The experimentally observed 'spacer effect' of such a hybrid material is well reproduced and further found to be particle-size sensitive. With the increase of nanoparticle size, the micro deformation mechanism will change from nanoparticles trapped in the graphene sheet, slipping on the graphene sheet, to aggregation outside the graphene sheet. Beyond a critical relative particle size 0.26, the graphene-sheet-dominated deformation mode changes to be a nanoparticle-dominated one. The final microstructure after compression of the hybrid system converges to two stable configurations of the 'sandwiched' and 'randomly-stacked' one. The results should be helpful not only to understand the micro mechanism of such a hybrid material in different applications, but also to the design of advanced composites and devices based on porous materials mixed with particles.

Supplementary material for this article is available [online](#)

\* Authors to whom any correspondence should be addressed.

Keywords: nanoparticle filled graphene foam material, uniaxial compression, mechanical property, micro deformation mechanism, coarse-grained molecular dynamics

(Some figures may appear in colour only in the online journal)

## 1. Introduction

Recently, with the rapid development of two-dimensional materials [1], such as graphene, molybdenum disulfide, boron nitride and so on, their three-dimensional assembly materials have attracted increasing attention in many fields, such as materials, physics, chemistry, biology, and even advanced engineering applications. Graphene foam (GrF) material, as a typical representative, possesses a multi-porous structure composed of randomly or regularly interconnected mono/bi/multilayered graphene sheets. Due to the combined advantage of porous materials and graphene sheet itself, graphene foam material has a host of excellent mechanical and physico-chemical properties, such as high tensile/compressive strength ( $\sim 1.6/13.7$  GPa) [2], super-wide density range ( $0.16\text{--}1580$  mg cm $^{-3}$ ) [3, 4], much high compressibility ( $\sim 98\%$ ) [5] and stretchability ( $\sim 70\%$ ) [6], high specific area ( $\sim 994.2$  m $^2$  g $^{-1}$ ) [7], superior thermal and chemical stability [8] and giant energy adsorption capacity ( $\sim 3400$  J g $^{-1}$ ) [9]. The extraordinary properties foster great research enthusiasm for a number of cutting-edge applications, such as advanced composite materials [10], highly-sensitive sensors [11], lithium ion batteries [12], even biomedical tissue engineering [13] and so on. All the applications are inevitably related to the mechanical properties of graphene foam materials.

In the past few years, extensive experimental, numerical, and theoretical investigations have been conducted to understand the underlying mechanisms of the mechanical properties of pristine graphene foam materials. Agarwal *et al* [14] conducted nano-indentation and *in situ* tensile test on graphene foam materials inside scanning electron microscopes (SEM) and found that the elastic modulus (69.9 GPa) in tension is four orders of magnitude higher than that (1.2–1.5 MPa) in compression. Gao *et al* [15] experimentally studied the size-dependent properties of GrFs assembled with flakes of different sizes ranging from sub-micron to tens of micrometer using the freeze casting technique, and found that the GrF with flakes of larger sizes showed both higher strength and fatigue resistance. Baimova *et al* [16] first investigated the GrFs subjected to the shear deformation and hydrostatic compression using full-atom molecular dynamics (FAMD) simulations and found that the shear deformation could alter both microstructures and mechanical properties of GrFs. Afterwards, with a 3D graphene coarse-grained (CG) model [17], Wang *et al* [18, 19] studied the microstructure deformation mechanism of GrFs under uniaxial compression, in which three major energy dissipation mechanisms were found, i.e. sliding, impacting and rippling of graphene sheets, and the deformation of GrFs was found to be dominated by the flake bending instead of stretching. Combining the transport modeling with coarse-grained molecular dynamics (CGMD), Liu *et al* [20] studied the critical phenomenon of the maximum conductivity of GrFs and explained its

competition mechanism. Pan *et al* [21, 22] investigated the mesostructure evolution of GrFs in tension and the super-elasticity of hole-flake GrFs in compression, in which it was found that the multi-peak stress–strain relationship is attributed to the collective bond breaking in tension and the mesoscopic criterion of abnormal increase of bead-bond length during supercompression was unveiled. Qin *et al* [23] combined FAMD simulations with experiments based on 3D-printed models and showed that GrFs have an exceptionally high ultimate tensile strength of 10 times as strong as mild steel, but with a relatively low density of 4.6% that of mild steel. Xia *et al* [8] adopted the CG model [24] of graphene sheets to study the temperature-dependent behavior of GrFs and found a fluid-like behavior similar to linear polymer melts at elevated temperatures and the transformation into a glassy-like ‘foam’ state at temperatures below the glass-transition temperature  $T_g$ .

Recently, different additives that are often in the form of nanoparticles (NPs) have been consciously introduced into the porous graphene foam material for specific functions. The interaction between particles and graphene sheets plays an important role in the realization of the special functions, which will inevitably affect the mechanical properties of graphene foam materials. The basic knowledge about the pristine GrFs is highly necessary, but not sufficient to thoroughly understand the mechanical properties of GrF-based composites. For example, many nanoscaled metal oxide particles, such as Fe $_3$ O $_4$  [25], CoO [26] and SnO $_2$  [27], are specifically added into GrFs, which can enhance the electrochemical lithium storage performance (e.g. a high reversible capacity of  $\sim 1000$  mAh g $^{-1}$ ) as an alternative anode material. Pd, Pt, Ni and Sn nanoparticles with higher loadings of 59, 67, 39 and 46 wt%, respectively, are added into GrFs, which can greatly improve the sensing performance of hydrogen gas with a response time of 25 s and a recovery time of 175 s over detection range of 100–1000 ppm [28–30]. In the flexible electronic device [31], Fe $_3$ O $_4$  magnetic nanoparticles are embedded into GrFs to achieve up to 52% reversible magnetic field-induced strain and strain-dependent electrical resistance. More examples are given in our comprehensive statistics in table S1 in supporting materials (available online at [stacks.iop.org/NANO/32/115701/mmedia](https://stacks.iop.org/NANO/32/115701/mmedia)). In the particle-rich hybrid systems, at least two intrinsic particle-induced effects on both structures and properties have been identified while not yet been seriously evaluated. It was found that entrapped NPs can effectively stop aggregation of graphene sheets due to the so-called ‘spacer effect’ [32], which consequently reaches a high specific surface area of composites [33]; however, as we know that NPs always prefer to aggregate on graphene sheets, which would in turn deteriorate the resulting performance of composite systems. A comprehensive examination is highly required to reconcile the two contradictory aspects for optimal design of GrF-based systems.

More importantly and generally, graphene foam material is a representative of the new polymer systems, which is assembled by paper-like ‘2D macromolecules’ [8, 34, 35] instead of the conventional linear ones [36]. When such a porous material assemblies with heterogeneous NPs, the interaction mode between paper-like sheets and NPs should be much different from that in the conventional linear polymer composite [37, 38]. Thus, to examine the basic physics and mechanics of GrF-NPs hybrid systems is really required to understand such a promising polymer composite system.

However, up to now, there is no theoretical/numerical work on the basic physics and mechanics of particle-modulated GrFs. Interaction between nanoparticles and graphene sheets remains unclear, which should be an important role in realizing different functions of such a hybrid material. It is still unclear which factors will affect the evolution of microstructures, and then affect the overall mechanical properties and deformed configurations.

In this work, CGMD simulations are carried out as numerical experiments to systematically investigate the mechanical properties and the corresponding micro deformation mechanism of particle-filled graphene foam materials under uniaxial compression, in which the effects of the size and volume fraction of NPs are mainly considered. Both the experimentally observed spacer effect and particle agglomeration phenomenon are well reproduced. The constitutive relation of nanoparticle filled graphene foam materials under uniaxial compression is achieved. The corresponding microstructural deformation and rearrangement are clearly revealed, which accompany with three kinds of microstructure behaviors, i.e. trapping, sliding and agglomeration of particles. The results in the present study could provide fundamental understanding of the mesoscopic mechanical nature of the particle-filled porous composites composed by 2D graphene sheets and be helpful for the optimal design of functional materials based on the mixture of nanoparticles and graphene sheets.

## 2. Numerical model of nanoparticle filled graphene foam materials

### 2.1. Mesoscopic CG method

In this paper, the mesoscopic CG scheme of graphene sheets is adopted, which was established by Cranford and Buehler [17] and well used in a series of studies on deformation mechanisms and mechanical properties of both graphene and pristine graphene foams [18–22, 39]. In this scheme, a  $2.5 \times 2.5 \text{ nm}^2$  graphene sheet is CG to be a single bead and a large piece of graphene layer is modeled by a set of discrete beads interconnected by both linear and angle springs. A harmonic spring potential  $\phi_T = k_T(r - r_0)^2/2$  is used to describe the axial stretching energy among all pairs of bonded particles, where  $k_T$  denotes a spring constant and  $r$  is the distance between two particles with an equilibrium distance  $r_0 = 2.5 \text{ nm}$ . A harmonic rotational-spring potential  $\phi_\varphi = k_\varphi(\varphi - \varphi_0)^2/2$  is used to describe the in-plane bending energy under shear deformation,

where  $k_\varphi$  denotes the spring constant related to the bending angle  $\varphi$  among three particles with a referenced equilibrium angle  $\varphi_0 = 90^\circ$ .  $\phi_\theta = k_\theta(\theta - \theta_0)^2/2$  denotes the out-of-plane bending energy with a spring constant  $k_\theta$ , where  $\theta$  denotes the bending angle among three particles with a referenced equilibrium value  $\theta_0 = 180^\circ$ . The van der Waals interaction between neighboring beads (nanoparticles and/or graphene sheets) is described by a similar Lennard-Jones potential  $\phi = 4\varepsilon((\sigma/r)^{12} - (\sigma/r)^6)$  with different parameter settings of  $\varepsilon$  and  $\sigma$ , where  $\varepsilon$  is a parameter determining the depth of the potential well,  $\sigma$  is a length scale parameter determining the zero-energy distance, and  $r$  is the bead-to-bead distance. The corresponding CG parameters for nanoparticles and/or graphene sheets are obtained based on the equivalent energy principle and systematic full atomic calculations, which are given in table S2.

The numerical 3D pristine graphene foam skeleton is constructed with 100 square CG sheets with the side length 50 nm and 400 beads in each one. The sheets are randomly distributed in a 3D box with the length, width and height about 178 nm, 170 nm and 180 nm, respectively. The nanoparticles are modeled by coarse grains as well with the tunable size and volume fraction. Considering that approximately spherical nanoparticles are used in experimental works as cited in table S1 and summarized in figure S1, the spherical bead is adopted to simulate the behaviors of nanoparticles for simplicity. The density of our numerical model is in range of  $180\text{--}240 \text{ mg cm}^{-3}$ , which is in line with the density range of experimental results, i.e.  $12\text{--}280 \text{ mg cm}^{-3}$  [40–42]. The relative density of our graphene foam model is  $\sim 8.9\%$  corresponding to the porosity 91.1%. A single sheet in real materials may contain 1–10 graphene layers [14, 43, 44]. Here, 8-layered sheets are mainly adopted and the effect of sheet layers on the mechanical response of pristine graphene foams can be found in the previous work [45]. All sheets in the numerical model are assumed to be identical for simplicity.

### 2.2. Numerical fabrication of nanoparticles-filled GrF samples

Mimicking the experimental self-assembly synthesis technique [25], all graphene sheets and nanoparticles are initially placed randomly in a big cubic box, then, NPT assembly technique is adopted to deal with the system with periodic boundary conditions in three directions as well as a constant room temperature 300 K and one barometric pressure. A time step 1 fs is adopted. As a result, the system shrinks gradually and finally reaches an equilibrium state at about 10 ns with a criterion that the total energy fluctuation converges to less than 1% as shown in figure S2.

Figure 1(a) shows our 3D numerical model of GrF-NPs composites. Paper-like 2D graphene sheets (blue) are randomly distributed and interconnected to form a porous matrix skeleton, inside which a number of NPs (green) adhere and deposit on each sheet. Five typical microstructural configurations composed by particles and sheets are shown in figure 1(b), including the randomly-distributing NPs on a sheet (figure 1(b-I)), multi-layered NPs stacking on a sheet (figure 1(b-II)), the V-shaped stacking NPs aggregated at the groove of neighboring sheets

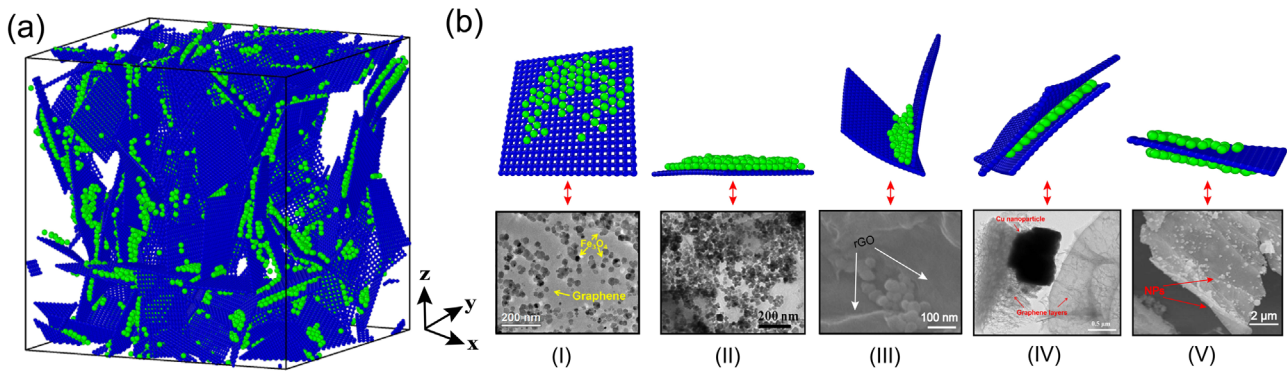


**Figure 1.** Schematics of 3D GrF-NPs composite materials and typical microstructures. (a) Relaxed configuration of a 3D GrF sample with NPs (green) adsorbed on the graphene sheets (blue); (b) five typical microstructural configurations in the GrF-NPs system in existing experiments by transmission electron microscope (TEM) and scanning electron microscope (SEM); (bottom) and our simulations (top): (I) a layer of NPs randomly adsorbed on a sheet reported in [31], copyright 2015 ACS; (II) multiple layers of NPs stacking on a sheet shown in [46] copyright 2020 Elsevier; (III) [47] reported NPs stacking near the point of contact between an edge and a surface, copyright 2020 Elsevier; (IV) NPs sandwiched between two sheets is explained in [48], copyright 2020 Elsevier; (V) [49] exhibit the NPs adsorbed on both sides of a sheet, MDPI Publisher (Open Acces).

(figure 1(b-III)), the NPs sandwiched between two sheets (figure 1(b-IV)) and a graphene sheet sandwiched between two layers of NPs (figure 1(b-V)). These typical configurations can be identified experimentally through TEM and SEM observations [31, 46–49] as the bottom subfigures shown in figure 1(b). It is very obvious that NPs act as spacers [25, 50] to prevent neighboring sheets from aggregating as observed in experiments and is well reproduced in our simulations as shown in figure 1(b) (III and IV). All these microstructures would show significant influence on the expected functions of nanoparticle-filled graphene foam materials. Furthermore, in such a nanoparticle-filled graphene foam system, nanoparticles have different states in different microstructures. It is much different from the microstructural feature in nanoparticle-filled carbon nanotube (CNT) networks [51, 52], where nanoparticles always prefer to gather at the junctions of CNT fibers.

To gain an in-depth understanding of the microscopic deformation mechanisms, microstructural evolution and stress–strain relationship, a series of numerical experiments under uniaxial compression are conducted on the present numerical GrF-NPs composite models. The compressive strain rate is set as  $\sim 5 \times 10^{-7} \text{ s}^{-1}$  in the  $x$  direction with a zero-pressure barostat in other two directions at room temperature. Periodic boundary conditions are used in all three directions. A time step of 1.0 fs is adopted in all the calculations. All the simulations are implemented using an open-source software Large scale Atomic/Molecular Massively Parallel Simulator [53]. The results are visualized based on Open Visualization Tool [54].

### 3. Results and discussion

#### 3.1. Size effect of NPs on the mechanical property and micro-deformation mechanism

The stress–strain curves of GrF-NPs composites with nanoparticles of different relative size  $D = d/L = 0.07, 0.26$  and  $0.5$ , but of the same volume fraction 27%, under uniaxial compression, are given in figure 2(a), where  $d$  and  $L$  denote the

diameter of nanoparticles and the side length of square graphene sheets, respectively. In comparison with the pristine graphene foam material, whose stress–strain curve exhibits a typical rubber-like feature with an initially elastic stage, a platform stage and the final compaction stage, the stress–strain curve of each GrF-NPs composite also approximately consists of three stages, i.e. an initially elastic stage with a compressive strain smaller than  $\sim 0.025$ , a weak strengthening stage and a strong strengthening stage. The elastic modulus  $E_{\text{init}}$  at the initial stage depends highly on the relative particle size  $D$ , as shown by the black line in figure 2(b), which increases slowly before a critical value of the initial elastic modulus  $E_{\text{init}}$  is about an order of magnitude higher than that of  $D < 0.07$ . Such a phenomenon should be due to the interaction between nanoparticles and graphene sheets. At the initial stage, the interaction between nanoparticles and sheets looks like discrete binders, which strengthen and stiffen the foam system. When the nanoparticle is relatively small, the influencing distance and the strength of binders should be relatively small, leading to a smaller initial modulus  $E_{\text{init}}$  of GrF-NPs composites. When the nanoparticle is relatively large, the influencing distance and the strength of binders should be relatively large, leading to a larger initial modulus  $E_{\text{init}}$ . As for the increasing intermediate modulus  $E_m$  within the compressive strain range of 0.18–0.50, the stress–strain curves of GrF-NPs composites gradually deviate from the rubber-like platform feature at the second stage. The intermediate modulus  $E_m$  is extracted and shown as a blue line in figure 2(b). Another critical relative particle size  $D_{c2} = \sim 0.26$  is found, below which the intermediate modulus  $E_m$  increases slightly and beyond which the intermediate modulus  $E_m$  increases sharply. A particle-size dependent effect exists, which further induces a deformation transformation mechanism. In order to explain such a phenomenon, we need to turn to the detailed microstructure evolution process and morphology.

Three typical snapshots of GrF materials filled with smaller NPs of  $D = 0.07$  and  $D = 0.50$  are recorded as shown in figures 2(c) and (d), respectively, which respectively correspond to the initial stage, the mediate stage of  $\varepsilon \sim 37\%$  and the final

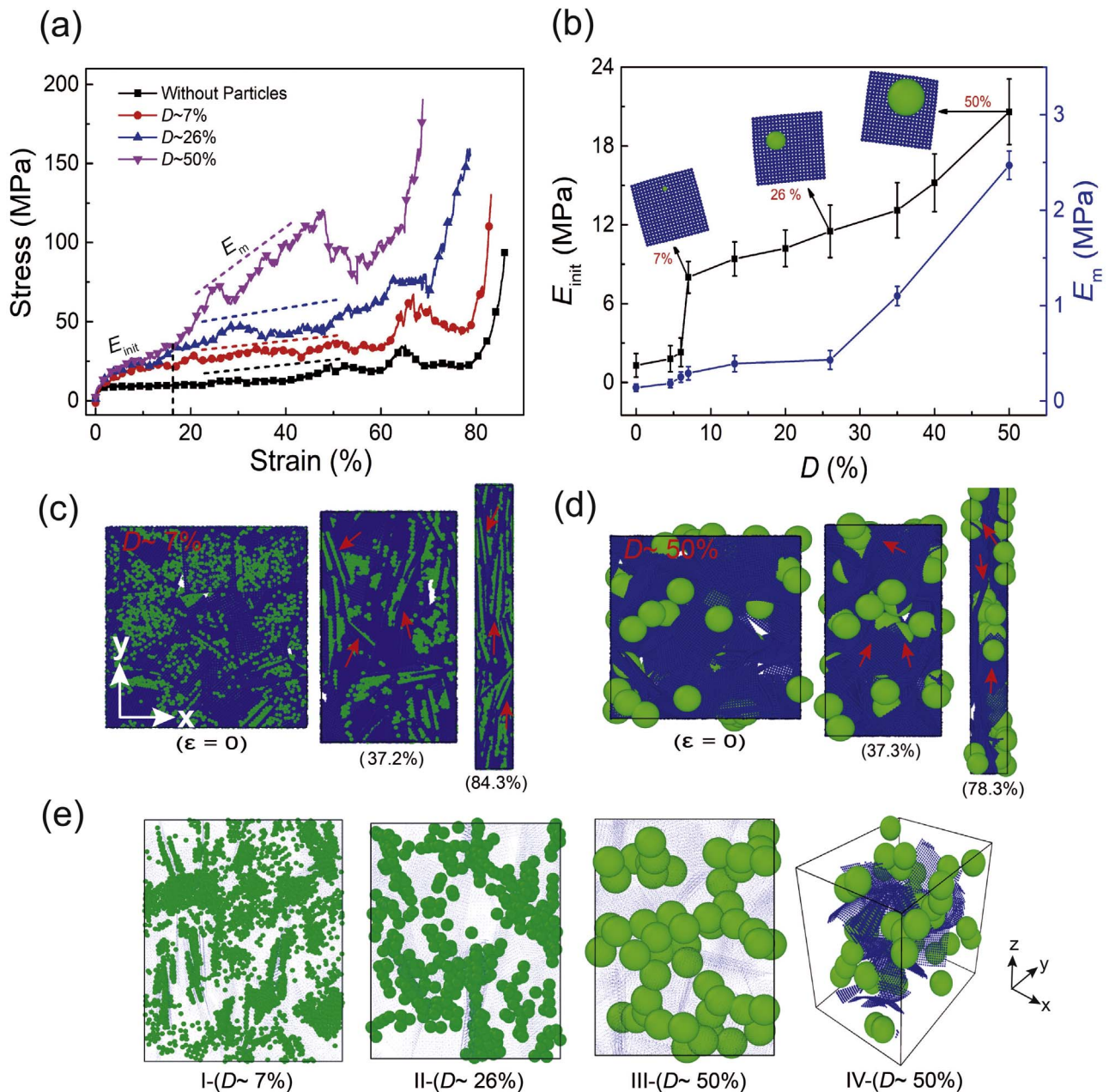


**Figure 2.** GrF-NPs hybrid composites under uniaxial compression. (a) The stress–strain relation of GrFs with varied relative particle diameters  $D$  of 0.07, 0.26 and 0.50 for a given volume fraction. Here  $D \equiv d/L$ ,  $d$  and  $L$  denote the diameter of nanoparticles and the side length of square graphene sheets, respectively; (b) the initial and intermediate modulus of GrF-NPs composites as a function of the relative particle diameter  $D$ ; (c), (d) three typical snapshots of GrF-NPs composites with  $D = 0.07$  and  $0.5$  under different compressive strain, respectively; (e) the structural skeletons of GrF materials filled with different sized nanoparticles at 0.2 compressive strain, in which the color of graphene sheets is lightened in (e-I-III) in order to highlight the structure of particle clusters, except for the compact laminated sheets among large particles in the loading direction as shown in (e-IV).

stage  $\epsilon \sim 80\%$ . Initially, smaller NPs (green dots) adhere on the graphene sheets and spread almost randomly and uniformly in the whole graphene foams as shown in figure 2(c). During compression, both the graphene sheets and NPs become a ‘sandwiched configuration’ as labeled by red arrows in figure 2(c), no matter how large the compressive strain is. Such a hybrid system is dominated by the deformation of graphene sheets, similar to that in a pristine graphene foam material [19, 45]. However, in the composites filled with larger NPs of  $D = 0.50$ , the microstructures are unstable during compression,

in which NPs separate from the original host sheets and aggregate in the system, forming a laminated graphene sheet structure with clustering particles, as labeled in red arrows in figure 2(d).

Skeletons of composites filled with NPs of different size at compressive strain of 0.2 are further shown in figure 2(e), in which the color of graphene sheets is lightened in order to highlight the structure of particles. It is clearly shown that, under compression, the larger the particle size, the easier it is to gather in the hybrid system. It means that, with the increase of nanoparticle size, the microscopic mechanism turns from

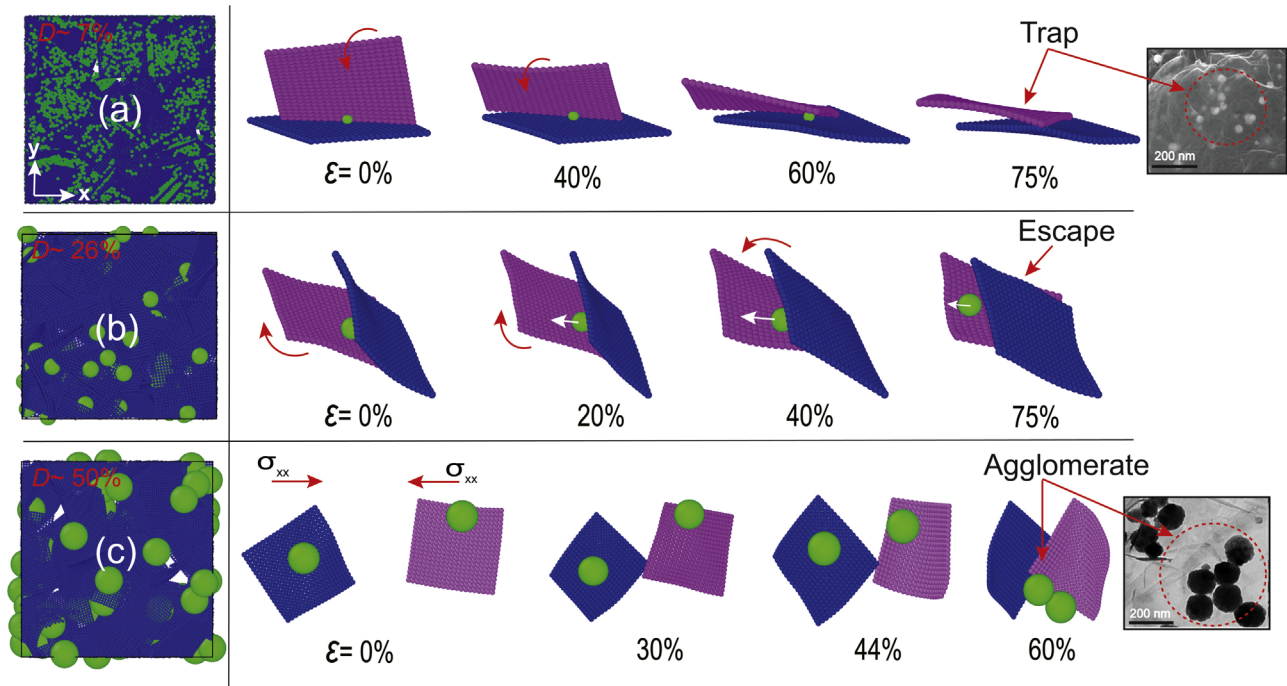


**Figure 3.** Microstructural evolution in GrF composites filled with nanoparticles of different size. (a) Small particles of  $D < 0.07$  are trapped between two neighboring sheets similar to the SEM observation of trapped Pt NPs under graphene sheets as explained in [55], copyright 2020 Elsevier; (b) medium sized particles of  $0.07 < D < 0.26$  will escape outward when two neighboring sheets are closed; (c) large particles of  $D > 0.26$  tend to agglomerate as observed in the SEM observation elucidated in [46], copyright 2020 Elsevier.

the deformation of graphene sheets with randomly adhered nanoparticles to the combination behavior of local aggregation of particles and the self-compactness of graphene sheets. Therefore, the experimentally observed ‘spacer effect’ [32] corresponds only to the case with relatively small nanoparticles, in which the final configuration is a ‘sandwiched’ one. In the present model, the corresponding critical size of nanoparticles is  $D_{c2} = \sim 0.26$ , below which ‘spacer effect’ exists.

The evolution images of microstructures with different sized particles are further given in figure 3. In the hybrid system with small nanoparticles of  $D < 0.07$  as shown in figure 3(a), the small particle adsorbs initially on a sheet. When the host sheet and the neighboring one deform under an external compression, the small particle remains still without feeling the effect of the external load. Consequently, in a hybrid system with a large number of small NPs, a ‘sandwiched’ structure will be formed, corresponding to the microscopic mechanism of deformation of graphene sheets with randomly adhered nanoparticles, which is much similar to that of a pristine GrF material [45] and the similar ‘trap’ configuration can be widely observed in the experiment [55] as the last sub-figure showing the trapped Pt nanoparticles under graphene sheets. In the hybrid system with mediate sized nanoparticles of  $0.07 < D < 0.26$  as shown in figure 3(b), the particle stays initially on a sheet. With the increase of external load, the particle starts to move when the two neighboring sheets come close. Finally, the particle escapes from the capture of two neighboring sheets. In the hybrid system with large nanoparticles of  $D > 0.26$  as shown in figure 3(c), particles are prone to agglomerating and graphene sheets will adsorb tightly

around large particles. To further clarify the atomic interaction of nanoparticles and graphene sheets, see the movies M1, M2 and M3 in supporting material. This agglomeration phenomenon has also been observed in recent report [46] as the last sub-figure shown in figure 3(c) about the large  $\text{Fe}_3\text{O}_4$  nanoparticles (up to  $\sim 140$  nm in diameter) on graphene nanosheets as a promising anode material for lithium batteries.

From above, it is known that the microstructural evolution affects the mechanical property of the hybrid material, which will subsequently affect the internal stress distribution. The spatial distributions of six independent local stress components  $\sigma_{xx}$ ,  $\sigma_{yy}$ ,  $\sigma_{zz}$ ,  $\sigma_{xy}$ ,  $\sigma_{xz}$  and  $\sigma_{yz}$  of the virial stress tensor  $\sigma$  are given in figure 4, which correspond to three GrF composites filled with nanoparticles of  $D = 0.07$ ,  $0.26$  and  $0.50$  under uniaxial compression in the  $x$ -axis direction, respectively. In the initial stage, the normal stress  $\sigma_{xx}$  for all three systems is relatively uniform as indicated by the green color in figures 4(a-I), (b-I) and (c-I). At the final stage with about 0.8 compressive strain in the  $x$ -axis direction as shown in figures 4(a-II), (b-II) and (c-II), it is found that the compressive stress  $\sigma_{xx}$  becomes more and more uneven with the increase of nanoparticle size, and larger particles will bear larger compressive load (dark blue). We further find that large particles of  $D = 0.50$  start to bear the major compressive load as early as the compressive strain reaches 0.2 as shown in figure S3 in supporting materials.

The distributions of the other five stress components in the three systems are much different from that of  $\sigma_{xx}$  and exhibit highly nonuniform distributions featured by the combination of tensile (red) and compressive (blue) stresses as shown in figures 4(a)(III–VII), (b)(III–VII) and (c)(III–VII). The average value of the five stress components should

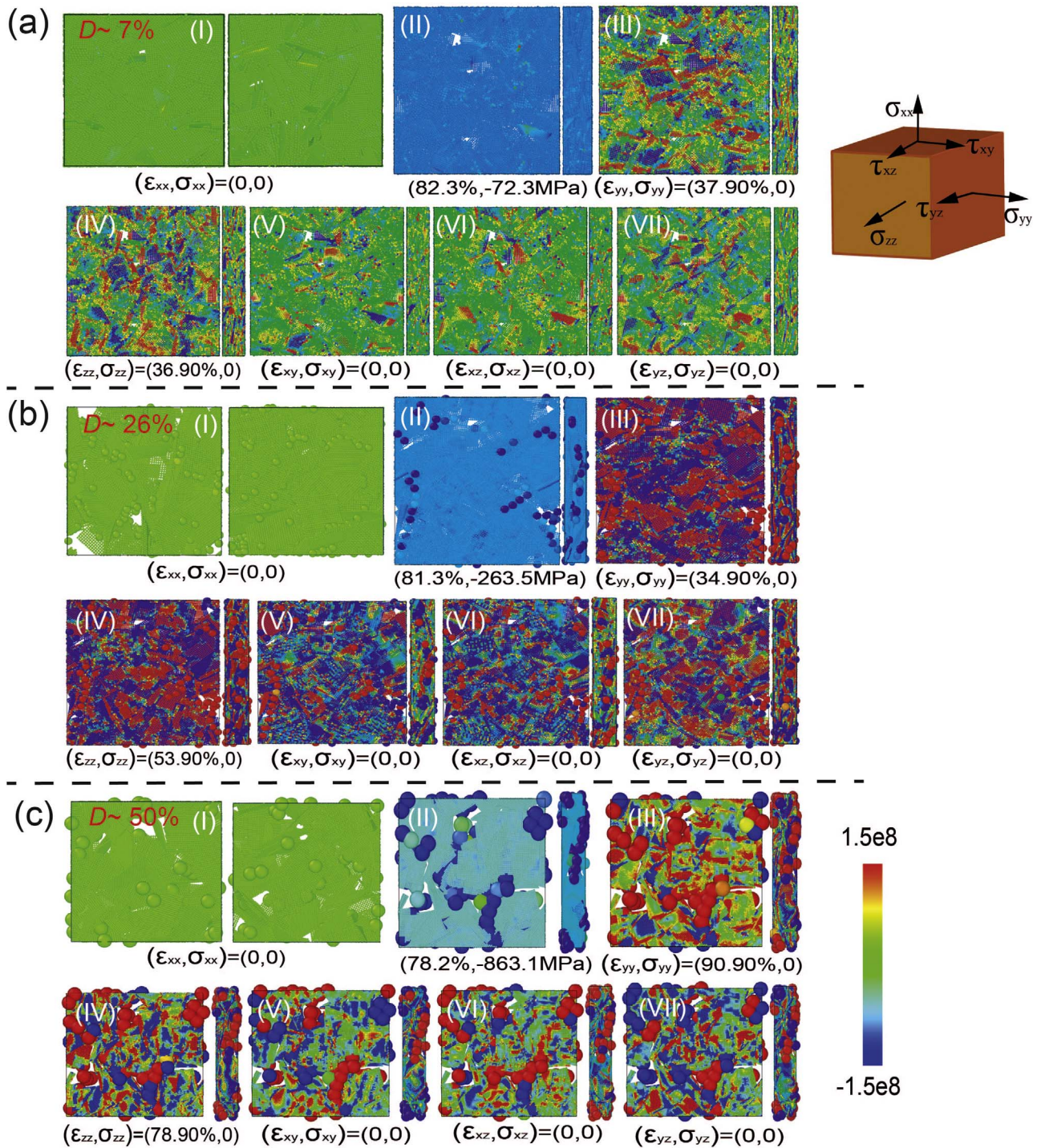


**Figure 4.** Local stress distribution of GrF-NPs systems under uniaxial compression at varied relative particle size  $D$ , (a) 7%, (b) 26% and (c) 50%, respectively. For each size, the  $\sigma_{xx}$  of both initial (subgraph I) and end (subgraph II) states are given. Other five independent stress components of  $\sigma_{yy}$ ,  $\sigma_{zz}$ ,  $\sigma_{xy}$ ,  $\sigma_{xz}$  and  $\sigma_{yz}$  are shown in the subgraph III–VII. In each subgraph, the left and right part is the top (compression direction) and side view, respectively. The continuum definition of six stress components is given in the right-top schematic diagram.

be zero due to the uniaxial compression condition. Moreover, no matter the normal stress or the shear stress, the larger the nanoparticle, the larger tensile or compressive stress it bears.

### 3.2. The effect of volume fraction of NPs on the mechanical property and micro-deformation mechanism

It can be inferred from above analysis that GrF composites filled with relatively small sized nanoparticles may be

advantageous in practical applications, since particle escaping and aggregation are generally not desirable in such a hybrid system. Therefore, we fix the relative size of nanoparticles as  $D = 0.06$  in this subsection to investigate the effect of volume fraction of nanoparticles on the mechanical property of GrF-NPs composite systems and the microscopic deformation mechanism under uniaxial compression.

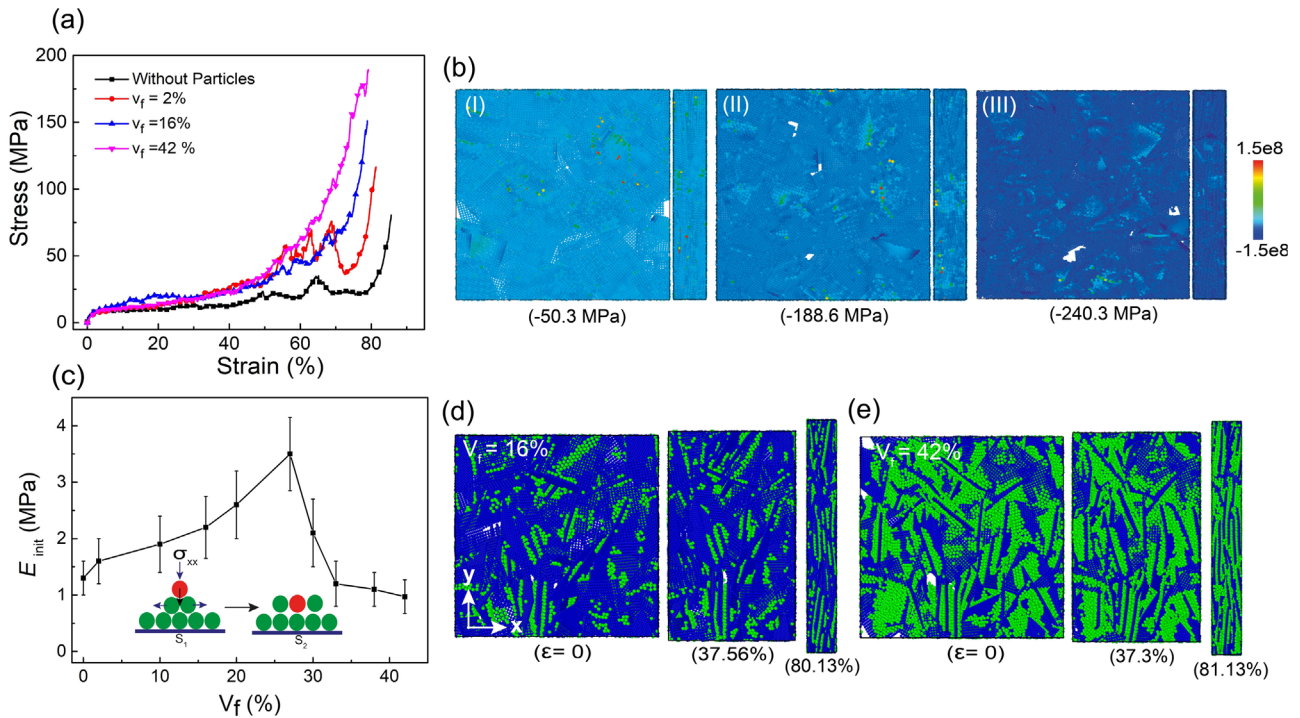


**Figure 5.** GrF-NPs composite systems with nanoparticles of a fixed size  $D = 0.06$  under uniaxial compression. (a) The stress–strain relation of GrF-NPs composite systems with different volume fractions of nanoparticles under uniaxial compression; (b) the distribution of  $\sigma_{xx}$  at the maximum compressive strain 0.80 in three different GrF-NPs composite systems with the particle volume fractions of (I) 2%, (II) 16% and (III) 42%, respectively. In each subgraph, the left and right part denote the top (compression direction) and side views, respectively; (c) the initial modulus of GrF-NPs composite systems as a function of the volume fraction of NPs; (d), (e) three typical snapshots of GrF-NPs composite systems with a respective particle volume fraction of 16% and 42% under compression.

The stress–strain relations of GrF-NPs systems with particle volume fractions of 2%, 16% and 42%, respectively, are shown in figure 5(a), all of which exhibit a rubber-like feature, similar to that of a pristine GrF material. Negligible difference remains till 0.5 compressive strain, which indicates that it is the graphene foam skeleton bearing the compressive load even if the volume fraction of nanoparticles gets to 42% in the foam system. The mechanical property becomes sensitive to the volume fraction when the compressive strain surpasses about 0.5. The compressive stress in the system with more NPs is larger than that with less NPs, which is more obviously shown in figure 5(b)(I–III) with the distributions of  $\sigma_{xx}$  in three systems at the maximum compressive strain. The initial modulus of GrF-NPs composites is also influenced by the volume fraction of nanoparticles as shown in figure 5(c), in which there exists a volume fraction of about 26%, corresponding to a maximum modulus. Such a phenomenon should be due to the local slip of particle pile. With the increase of volume fraction of NPs, more and more particles adhere on the graphene sheets, which should improve the modulus of graphene sheets. However, when the volume fraction of nanoparticles is large enough, nanoparticle piles will form on the graphene sheets. Local slipping of single particle or neighboring particle layers will happen under the external compression, which would decrease the modulus of the composite due to the weak interface among NPs according to the composite material theory [56]. Three typical snapshots for GrF-NPs composites with a respective

volume fraction of 16% and 42% under different compressive strain are shown in figures 5(d) and (e), respectively. It is clearly shown that nanoparticle piles form in the composite system filled with a large volume fraction of nanoparticles, which has a poor local shear capacity.

Typical microstructures and their evolution in the composite system with nanoparticles of 42% volume fraction and  $D = 0.06$  are shown in figure 6. The initial configuration is shown in figure 6(a-I), where it is found the initial microstructures consist of particles stacked on both sides of graphene sheets (left-top), clustered randomly on the surface of sheet (left-bottom), trapped between V-shaped joint of two sheets (right-top), and laminated between two layered sheets (right-bottom). Under compression, each microstructure evolves continuously. All the processes are mainly due to the particle slipping and rotating. Two stable microstructures are finally formed as shown in figure 6(a-II), in which one is a ‘sandwiched’ structure and the other is a ‘randomly-stacked’ one. The corresponding evolution processes of the two structures are given in figures 6(b) and (c), respectively. It is clearly shown that a pile of particles initially stacked in the junction of two sheets are squeezed out gradually and spread out on sheets to form the ‘sandwiched’ structure. During the forming process of the ‘randomly-stacked’ structure as shown in figure 6(c), some NPs initially stay on the sheet ‘3’. Under compressive strain, sheets ‘1’ and ‘2’ come close, which accumulate the particles arbitrarily to form a randomly-stacked structure trapped among three contact sheets. The

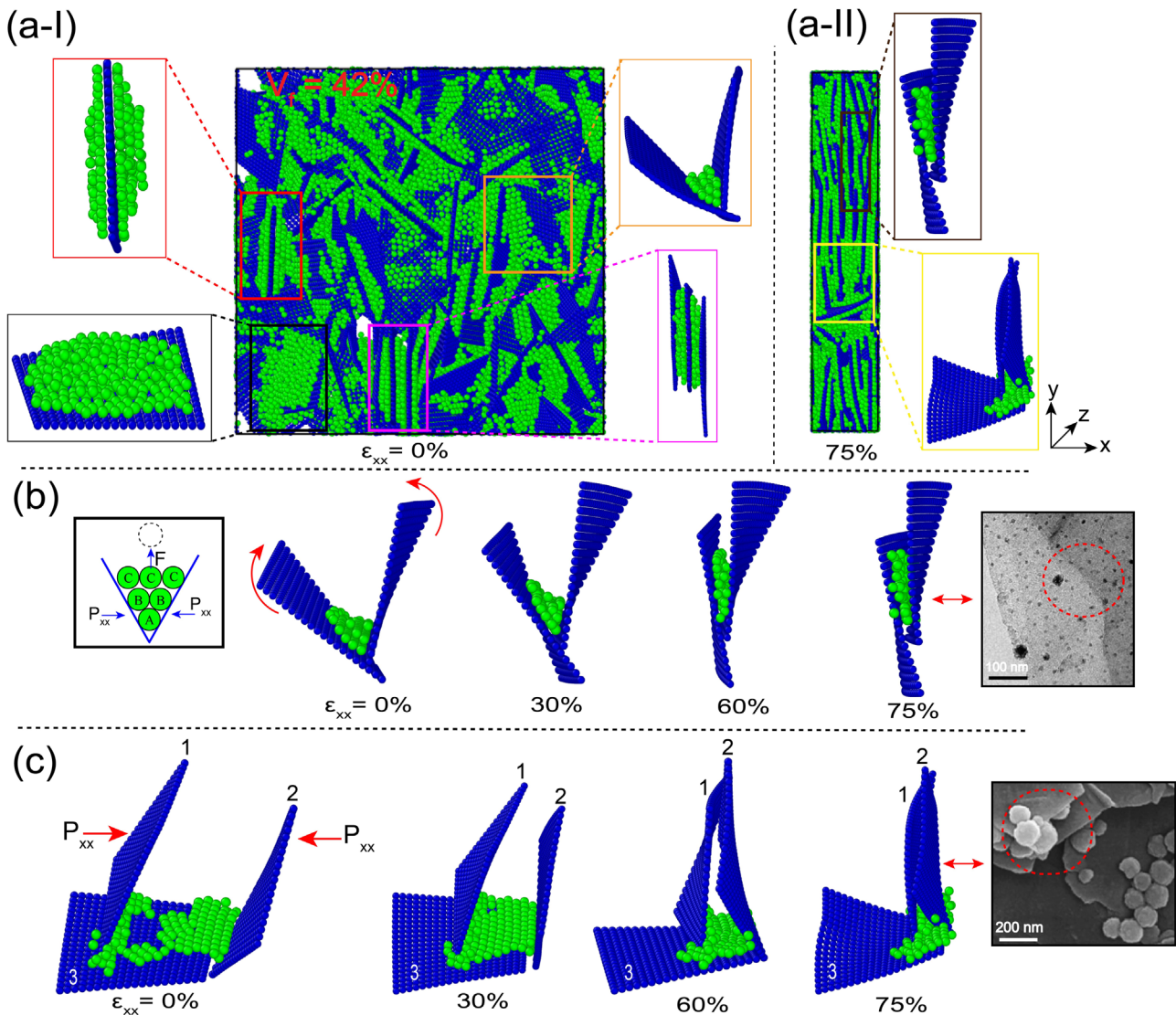


**Figure 6.** Particle distributions and microstructural evolution in GrF-NPs composites filled with 42% volume fraction of nanoparticles. (a-I) Typical distributions of nanoparticles in GrF: bi/tri-layers of nanoparticles stacked (left top) or clustered (left down) on a sheet; a pile of nanoparticles agglomerating between V-shaped region of multiple sheets (right top) or sandwiched between laminated sheets (right down); (a-II) sandwiched and randomly-stacked nanoparticles after compression with compressive strain of 75%; (b) the forming process of a sandwiched structure, during which the stacked particles are squeezed out gradually when the two sheets come close under compression; [57] explained the SEM image of two sheets having sandwiched structure with squeezed particles, copyright 2019 RSC; (c) a randomly-stacked structure forming at the junction of multiple sheets under compression; SEM image of NPs on randomly-stacked graphene sheets as explained in [46], copyright 2020 Elsevier.

corresponding two types of microstructures are observed as well in experiments [57] as given in figures 6(b), (d) for comparison.

#### 4. Conclusions

In this paper, the mechanical property and its microscopic deformation mechanism of nanoparticle-filled graphene foam materials under uniaxial compression are systematically investigated with CGMD simulation method, in which effects of the size and volume fraction of nanoparticles on the stress-strain relation and microstructural evolution are considered.

The initial numerical model is in good agreement with the experimental samples, containing typical microstructures, i.e. the randomly-distributed single layer of NPs on graphene sheets, multi-layered NP accumulation, aggregation of nanoparticles at V-shaped grooves forming by neighboring sheets. Under compression, the initial microstructures evolve continuously through the interaction between particles and graphene sheets. The ‘spacer effect’ and ‘aggregation effect’ have been well reproduced in the simulations, consistent with experimental observations.

With the increase of nanoparticle size, the particle-size-dependent evolution process changes from particles adhering to the sheet, sliding on the sheet, to aggregating locally. As a

result, the deformation mode changes from the graphene-sheet-dominated mechanism to the nanoparticle-dominated one. The mechanical property of such a hybrid material is further affected. Two critical sizes of nanoparticles exist. The first one is  $D_{c1} = \sim 0.07$ , below which the initial modulus changes slightly with the increase of nanoparticle size, and beyond which the initial modulus varies very quickly with the increase of nanoparticle size. The second one is  $D_{c2} = \sim 0.26$ , below which the intermediate modulus increases slightly with the nanoparticle size, and beyond which it increases quickly.

Variation of the volume fraction of relatively small nanoparticles does not show significant effect on the stress-strain relation of the hybrid composite, which is still similar to that of rubber-like materials with an elastic stage, a platform stage and a compaction stage. With the increase of volume fraction of nanoparticles, more and more nanoparticles adhere on the graphene sheets, yielding an improved initial modulus of the composite. However, a critical volume fraction of about 26% exists, beyond which the initial modulus of the composite decreases due to the interlayer slip of multi-layered nanoparticles and nanoparticle piles. The final microstructures converge to a 'sandwiched' configuration and a particle 'randomly-stacked' structure.

The results in this study should be helpful not only to understand the microscopic deformation mechanism of such a special composite, but also to the design of advanced functional devices based on nanoparticle-filled foam materials.

## Acknowledgments

The work reported here is supported by NSFC through Grants #11872114, #11532013, #11972348, #12002034, Strategic Priority Research Program of the Chinese Academy of Sciences (Grants No. XDB22040503) and the CAS/SAFEA International Partnership Program for Creative Research Teams.

## Author contributions

S H C and C W conceived the original idea, designed and supervised the simulations. M B K formulated the numerical model, conducted all simulations and drafted the paper. S H C and C W revised the manuscript. All authors reviewed and contributed to the paper.

## Notes

The authors declare no competing interest.

## ORCID iDs

Muhammad Bilal Khan  <https://orcid.org/0000-0002-8316-3002>

Chao Wang  <https://orcid.org/0000-0002-3234-6917>

## References

- [1] Mas-Balleste R, Gomez-Navarro C, Gomez-Herrero J and Zamora F 2011 2D materials: to graphene and beyond *Nanoscale* **3** 20–30
- [2] Zhang X, Zhong L, Mateos A, Kudo A, Vyatskikh A, Gao H, Greer J R and Li X 2019 Theoretical strength and rubber-like behaviour in micro-sized pyrolytic carbon *Nat. Nanotechnol.* **14** 762–9
- [3] Qiu L, Huang B, He Z, Wang Y, Tian Z, Liu J Z, Wang K, Song J, Gengenbach T R and Li D 2017 Extremely low density and super-compressible graphene cellular materials *Adv. Mater.* **29** 1701553
- [4] Tao Y, Xie X, Lv W, Tang D-M, Kong D, Huang Z, Nishihara H, Ishii T, Li B and Golberg D 2013 Towards ultrahigh volumetric capacitance: graphene derived highly dense but porous carbons for supercapacitors *Sci. Rep.* **3** 2975
- [5] Wu Y, Yi N, Huang L, Zhang T, Fang S, Chang H, Li N, Oh J, Lee J A and Kozlov M 2015 Three-dimensionally bonded spongy graphene material with super compressive elasticity and near-zero Poisson's ratio *Nat. Commun.* **6** 6141
- [6] Jeong Y R, Park H, Jin S W, Hong S Y, Lee S S and Ha J S 2015 Highly stretchable and sensitive strain sensors using fragmented graphene foam *Adv. Funct. Mater.* **25** 4228–36
- [7] Xu X, Guan C, Xu L, Tan Y H, Zhang D, Wang Y, Zhang H, Blackwood D J, Wang J and Li M 2019 Three dimensionally free-formable graphene foam with designed structures for energy and environmental applications *ACS Nano* **14** 937–47
- [8] Xia W, Vargas-Lara F, Keten S and Douglas J F 2018 Structure and dynamics of a graphene melt *ACS Nano* **12** 5427–35
- [9] Yi L, Chang T, Feng X-Q, Zhang Y, Wang J and Huang B 2017 Giant energy absorption capacity of graphene-based carbon honeycombs *Carbon* **118** 348–57
- [10] Chen Y, Dai G and Gao Q 2019 Starch nanoparticles-graphene aerogels with high supercapacitor performance and efficient adsorption *ACS Sustain. Chem. Eng.* **7** 14064–73
- [11] Zhao B, Sun T, Zhou X, Liu X, Li X, Zhou K, Dong L and Wei D 2019 Three-dimensional graphene composite containing graphene-SiO<sub>2</sub> nanoballs and its potential application in stress sensors *Nanomaterials* **9** 438
- [12] Qiu B, Xing M and Zhang J 2014 Mesoporous TiO<sub>2</sub> nanocrystals grown *in situ* on graphene aerogels for high photocatalysis and lithium-ion batteries *J. Am. Chem. Soc.* **136** 5852–5
- [13] Nieto A, Dua R, Zhang C, Boesl B, Ramaswamy S and Agarwal A 2015 Three dimensional graphene foam/polymer hybrid as a high strength biocompatible scaffold *Adv. Funct. Mater.* **25** 3916–24
- [14] Nieto A, Boesl B and Agarwal A 2015 Multi-scale intrinsic deformation mechanisms of 3D graphene foam *Carbon* **85** 299–308
- [15] Gao W, Zhao N, Yao W, Xu Z, Bai H and Gao C 2017 Effect of flake size on the mechanical properties of graphene aerogels prepared by freeze casting *RSC Adv.* **7** 33600–5
- [16] Baimova A, Korznikova E, Dmitriev S, Liu B and Zhou K 2014 REVIEW ON CRUMPLED GRAPHENE: UNIQUE MECHANICAL PROPERTIES *Rev. Adv. Mater. Sci.* **39** 69–83
- [17] Cranford S and Buehler M J 2011 Twisted and coiled ultralong multilayer graphene ribbons *Modelling Simul. Mater. Sci. Eng.* **19** 054003
- [18] Wang C, Pan D and Chen S 2018 Energy dissipative mechanism of graphene foam materials *Carbon* **132** 641–50
- [19] Wang C, Zhang C and Chen S 2019 Micro-mechanism and influencing factors of graphene foam elasticity *Carbon* **148** 267–76
- [20] Liu F, Wang C and Tang Q 2018 Conductivity maximum in 3D graphene foams *Small* **14** 1801458

- [21] Pan D, Wang C, Wang T-C and Yao Y 2017 Graphene foam: uniaxial tension behavior and fracture mode based on a mesoscopic model *ACS Nano* **11** 8988–97
- [22] Pan D, Wang C and Wang X 2018 Graphene foam: hole-flake network for uniaxial supercompression and recovery behavior *ACS Nano* **12** 11491–502
- [23] Qin Z, Jung G S, Kang M J and Buehler M J 2017 The mechanics and design of a lightweight three-dimensional graphene assembly *Sci. Adv.* **3** e1601536
- [24] Ruiz L, Xia W, Meng Z and Keten S 2015 A coarse-grained model for the mechanical behavior of multi-layer graphene *Carbon* **82** 103–15
- [25] Wang Y, Jin Y, Zhao C, Pan E and Jia M 2018 Fe<sub>3</sub>O<sub>4</sub> nanoparticle/graphene aerogel composite with enhanced lithium storage performance *Appl. Surf. Sci.* **458** 1035–42
- [26] Pan E, Jin Y, Wang Y, Zhao C, Bo X and Jia M 2018 Facile synthesis of mesoporous 3D CoO/nitrogen-doped graphene aerogel as high-performance anode materials for lithium storage *Microporous Mesoporous Mater.* **267** 93–9
- [27] Li L, He S, Liu M, Zhang C and Chen W 2015 Three-dimensional mesoporous graphene aerogel-supported SnO<sub>2</sub> nanocrystals for high-performance NO<sub>2</sub> gas sensing at low temperature *Anal. Chem.* **87** 1638–45
- [28] Shen C, Barrios E, McInnis M, Zuyus J and Zhai L 2017 Fabrication of graphene aerogels with heavily loaded metallic nanoparticles *Micromachines* **8** 47
- [29] Juanjuan Z, Ruiyi L, Zaijun L, Junkang L, Zhiguo G and Guangli W J N 2014 Synthesis of nitrogen-doped activated graphene aerogel/gold nanoparticles and its application for electrochemical detection of hydroquinone and o-dihydroxybenzene *Nanoscale* **6** 5458–66
- [30] Liu X, Cui J, Sun J and Zhang X 2014 3D graphene aerogel-supported SnO<sub>2</sub> nanoparticles for efficient detection of NO<sub>2</sub> *RSC Adv.* **4** 22601–5
- [31] Xu X, Li H, Zhang Q, Hu H, Zhao Z, Li J, Li J, Qiao Y and Gogotsi Y 2015 Self-sensing, ultralight, and conductive 3D graphene/iron oxide aerogel elastomer deformable in a magnetic field *ACS Nano* **9** 3969–77
- [32] Chen W, Li S, Chen C and Yan L 2011 Self-assembly and embedding of nanoparticles by *in situ* reduced graphene for preparation of a 3D graphene/nanoparticle aerogel *Adv. Mater.* **23** 5679–83
- [33] Ma Y, Younesi R, Pan R, Liu C, Zhu J, Wei B and Edström K 2016 Constraining Si particles within Graphene Foam Monolith: interfacial modification for high-performance Li+ storage and flexible integrated configuration *Adv. Funct. Mater.* **26** 6797–806
- [34] Bieri M, Nguyen M-T, Gröning O, Cai J, Treier M, Ait-Mansour K, Ruffieux P, Pignedoli C A, Passerone D and Kastler M 2010 Two-dimensional polymer formation on surfaces: insight into the roles of precursor mobility and reactivity *J. Am. Chem. Soc.* **132** 16669–76
- [35] Knauert S T, Douglas J F and Starr F W 2010 Morphology and transport properties of two-dimensional sheet polymers *Macromolecules* **43** 3438–45
- [36] De Gennes P-G 1990 *Introduction to Polymer Dynamics* (USA: Cambridge University Press (CUP))
- [37] Li Y, Kröger M and Liu W K 2012 Nanoparticle effect on the dynamics of polymer chains and their entanglement network *Phys. Rev. Lett.* **109** 118001
- [38] Li Y, Kröger M and Liu W K 2012 Nanoparticle geometrical effect on structure, dynamics and anisotropic viscosity of polyethylene nanocomposites *Macromolecules* **45** 2099–112
- [39] Shang J J, Yang Q-S, Liu X and Wang C 2018 Compressive deformation mechanism of honeycomb-like graphene aerogels *Carbon* **134** 398–410
- [40] Kang W, Cui Y, Qin L, Yang Y, Zhao Z, Wang X and Liu X 2020 A novel robust adsorbent for efficient oil/water separation: magnetic carbon nanospheres/graphene composite aerogel *J. Hazard. Mater.* **392** 122499
- [41] Shi Y, Gao X and Qiu J 2019 Synthesis and strengthened microwave absorption properties of three-dimensional porous Fe<sub>3</sub>O<sub>4</sub>/graphene composite foam *J. Ceram. Int.* **45** 3126–32
- [42] Li J, Yang S, Jiao P, Peng Q, Yin W, Yuan Y, Lu H, He X and Li Y 2020 Three-dimensional macroassembly of hybrid C@CoFe nanoparticles/reduced graphene oxide nanosheets towards multifunctional foam *Carbon* **157** 427–36
- [43] Chen Z, Ren W, Gao L, Liu B, Pei S and Cheng H-M 2011 Three-dimensional flexible and conductive interconnected graphene networks grown by chemical vapour deposition *Nat. Mater.* **10** 424
- [44] Dienwiebel M, Verhoeven G S, Pradeep N, Frenken J W, Heimberg J A and Zandbergen H W 2004 Superlubricity of graphite *Phys. Rev. Lett.* **92** 126101
- [45] Wang C, Zhang C and Chen S 2016 The microscopic deformation mechanism of 3D graphene foam materials under uniaxial compression *Carbon* **109** 666–72
- [46] Gu S and Zhu A 2020 Graphene nanosheets loaded Fe<sub>3</sub>O<sub>4</sub> nanoparticles as a promising anode material for lithium ion batteries *J. Alloys Compd.* **813** 152160
- [47] Wang X, Lu Y, Zhu T, Chang S and Wang W 2020 CoFe<sub>2</sub>O<sub>4</sub>/N-doped reduced graphene oxide aerogels for high-performance microwave absorption *J. Chem. Eng.* **388** 124317
- [48] Zhang Y, Li N, Xiang Y, Wang D, Zhang P, Wang Y, Lu S, Xu R and Zhao J 2020 A flexible non-enzymatic glucose sensor based on copper nanoparticles anchored on laser-induced graphene *Carbon* **156** 506–13
- [49] Yuan H, Qi F, Zhao N, Wan P, Zhang B, Xiong H, Liao B and Ouyang X 2020 Graphene oxide decorated with titanium nanoparticles to reinforce the anti-corrosion performance of epoxy coating *Coatings* **10** 129
- [50] Ma J, He Y-S, Zhang W, Wang J, Yang X, Liao X-Z and Ma Z-F 2015 An experimental insight into the advantages of *in situ* solvothermal route to construct 3D graphene-based anode materials for lithium-ion batteries *Nano Energy* **16** 235–46
- [51] Wang C, Wang L and Xu Z 2013 Enhanced mechanical properties of carbon nanotube networks by mobile and discrete binders *Carbon* **64** 237–44
- [52] Liu Q, Li M, Gu Y, Wang S, Zhang Y, Li Q, Gao L and Zhang Z 2015 Interlocked CNT networks with high damping and storage modulus *Carbon* **86** 46–53
- [53] Plimpton S 1993 *Fast Parallel Algorithms for Short-Range Molecular Dynamics* (Albuquerque, NM: Sandia National Laboratories)
- [54] Stukowski A 2010 Visualization and analysis of atomistic simulation data with OVITO-the open visualization tool modelling *Modelling Simul. Mater. Sci. Eng.* **18** 015012
- [55] Zhou D, Jiang B, Yang R, Hou X and Zheng C 2020 One-step synthesis of monodispersed Pt nanoparticles anchored on 3D graphene foams and its application for electrocatalytic hydrogen evolution *J. Chin. Chem. Lett.* **31** 1540–4
- [56] Davies W 1971 The theory of elastic composite materials *J. Phys. D: Appl. Phys.* **4** 1325
- [57] Zhuang M, Liu Z, Ding Y, Xu G-L, Li Y, Tyagi A, Zhang X, Sun C-J, Ren Y and Ou X 2019 Methacrylated gelatin-embedded fabrication of 3D graphene-supported Co<sub>3</sub>O<sub>4</sub> nanoparticles for water splitting *Nanoscale* **11** 6866–75